ISSN 1392–1320 MATERIALS SCIENCE (MEDŽIAGOTYRA). Vol. 18, No. 1. 2012

Microstructure vs. Near-threshold Fatigue Crack Growth Behavior of an Heat-treated Ductile Iron

Radomila KONEČNÁ [1 *], Lukáš BUBENKO [1], Gianni NICOLETTO [2]

[1] *Department of Materials Engineering, University of Žilina, Univerzitná 1, 01026 Žilina, Slovak Republic*
[2] *Department of Industrial Engineering, University of Parma, Viale G.P. Usberti 181/A, 43100 Parma, Italy*

crossref http://dx.doi.org/10.5755/j01.ms.18.1.1336

Received 03 June 2011; accepted 09 July 2011

Perferritic isothermal ductile iron (IDI®) is an intermediate grade between the low-strength grades of austempered ductile iron (ADI) and pearlitic ductile iron (DI) recently developed by Zanardi Fonderie Italy. IDI is produced by heat-treating an unalloyed nodular cast iron. The specific matrix microstructure is called "Perferritic" and consists predominantly of ferrite and pearlite. Compared to the pearlitic grades of nodular ductile iron, IDI combines similar strength with higher toughness as a result of the isothermal heat treatment.

In this contribution the fatigue crack growth resistance and K_{ath} of IDI are investigated and correlated to mechanical properties and microstructural features. The threshold K_a was determined using the load shedding technique as per ASTM Standard E-647 using CT specimens extracted from a cast block. Tensile specimens were extracted from the broken CT halves and used to determine the static mechanical properties. A metallographic investigation was carried out to correlate structural features and mechanical properties.

Keywords: perferritic IDI, fatigue crack propagation, threshold stress intensity, tensile test, microstructure.

1. INTRODUCTION

Nodular cast iron (NCI) is a construction material widely used in many demanding technical applications, [1]. Its mechanical and fatigue properties can be significantly improved by a post-cast heat treatment, such as austempering. Austempered ductile iron (ADI), the result of an austempering treatment, represents the top grade of the NCI family range [2, 3]. However, the cost increase of alloying elements used in the low-strength ADI grades has led to a slow growth rate of new ADI applications in recent years and created the opportunity for the invention of Perferritic Isothermal Ductile Iron (IDI) [4].

Perferritic IDI is an intermediate grade between the low-strength ADI grades and the pearlitic DI. Compared with the pearlitic DI grades, IDI combines similar strength with higher toughness properties as a result of the isothermal heat treatment, performed after casting of a special preconditioning of the metal bath. The heat treatment basically consists of heating the DI casting above the critical temperature followed by cooling at a rate that promotes the pearlite formation. In addition, no alloying elements are added for the IDI production, thus benefiting in terms of cost, as well as in the technical performance, because the absence of alloying elements (Mo in particular) implies less segregation and as a consequence lower thickness sensitivity. The resulting microstructure of IDI predominantly consists of ferrite and pearlite, with different distribution compared to the as-cast DI, and graphite nodules. The IDI matrix is denominated "Perferritic" [4].

IDI development needs a high level of process integration starting from the design to the machining phase [4]. In general, IDI castings are proposed for service under dynamic variable loading. Understanding its properties, especially in case of fatigue design is thus necessary.

In contrast to the traditional stress-life approach to fatigue, the fracture mechanics approach assumes that cracks exist in materials and structures [5]. Use of crack propagation laws based on stress intensity factor K is then used to predict the service life of the component. Experimental characterization of fatigue crack growth behavior of a material leads to the determination of the relationship between fatigue crack propagation rate da/dN and the stress intensity factor amplitude K_a or stress intensity factor range ΔK. For intermediate crack growth rates, typically in the range of $10^{-6} - 10^{-3}$ mm/cycle and often called Paris region, the $\log(\mathrm{d}a/\mathrm{d}N)$ *vs.* $\log K_a$ dependence can be approximated by a straight line. At the low values of K_a, the crack propagation curve tends to the threshold value of stress intensity factor amplitude K_{ath}. Below this threshold, the fatigue crack will not propagate [6].

The very slow crack growth rates region and the threshold region are most important from the engineering point of view. A fatigue crack propagation curve representative of these two regions is given by the equation [6]:

$$da/dN = A\left(K_a^m - K_{ath}^m\right). \quad (1)$$

Parameters A and m as well as the threshold value K_{ath} depend on the stress ratio [6].

Fatigue crack propagation curves, $\mathrm{d}a/\mathrm{d}N$ vs. K_a, and the threshold amplitudes of fatigue crack propagation factor K_{ath} have been experimentally determined in this work using three identical compact tension (CT) specimens of IDI [7]. Since the resulting fatigue crack propagation characteristics showed considerable difference at low crack growth rates, a detailed microstructural analysis and static tests using tensile specimens extracted from the broken CT

*Corresponding author. Tel.: +421-41-5132604; fax.: +421-41-5652940.
E-mail address: *radomila.konecna@fstroj.uniza.sk* (R. Konečná)

halves have been consequently performed to investigate possible influencing factors.

2. EXPERIMENT

2.1. Material

The experimental material is a perferritic IDI supplied in the form of cast block ($75 \times 60 \times 160$ mm) by Italian company Zanardi Fonderie. Chemical composition of basic NCI according to the company is presented in Table 1.

Table 1. Chemical composition of NCI in weight %

C	Si	Mn	Cu	Ni	Mo
3.69	2.53	0.17	0.08	0.05	0.012

The distribution of graphite nodules, shown within non etched structure of IDI in Fig. 1, a, is almost uniform respecting eutectic crystallization and formation of eutectic cells [8] visible in Fig. 1, b. The graphite particles have nodular shape partly perfectly nodular with different size which will be subsequently described. The microstructure of NCI matrix after heat treatment consists of a mixture of proeutectoid ferrite and pearlite, denominated perferritic IDI. The typical microstructure of perferritic IDI is given in Fig. 1, c. Large regions with high volume of pearlite were present on the borders of the eutectic cells. Cast shrinkages were also typically observed, Fig. 1, d.

2.2. Methodology

Fatigue crack propagation experiments were performed according to the ASTM standard E 647-08 [7]. CT specimens, Fig. 2, with the thickness $B = 10$ mm and the width $W = 50$ mm and a chevron notch were machined from the supplied cast block. To provide sufficient visibility of fatigue crack propagation, lateral specimen surfaces were polished by 1 micron grain size diamond paste. CCD cameras were applied to monitor the propagating cracks, while the current crack length (a) was measured by digital micrometers and recorded simultaneously with number of cycles (N).

Both the precracking and crack propagation tests were performed in the electromagnetic resonant testing machine Roell Amsler HFP 5100 at initial cyclic frequency of 100 Hz. A sinusoidal waveform with the constant load ratio $R = 0.1$ was applied.

Three CT specimens were tested and the fatigue crack propagation curves da/dN vs. K_a were determined [7].

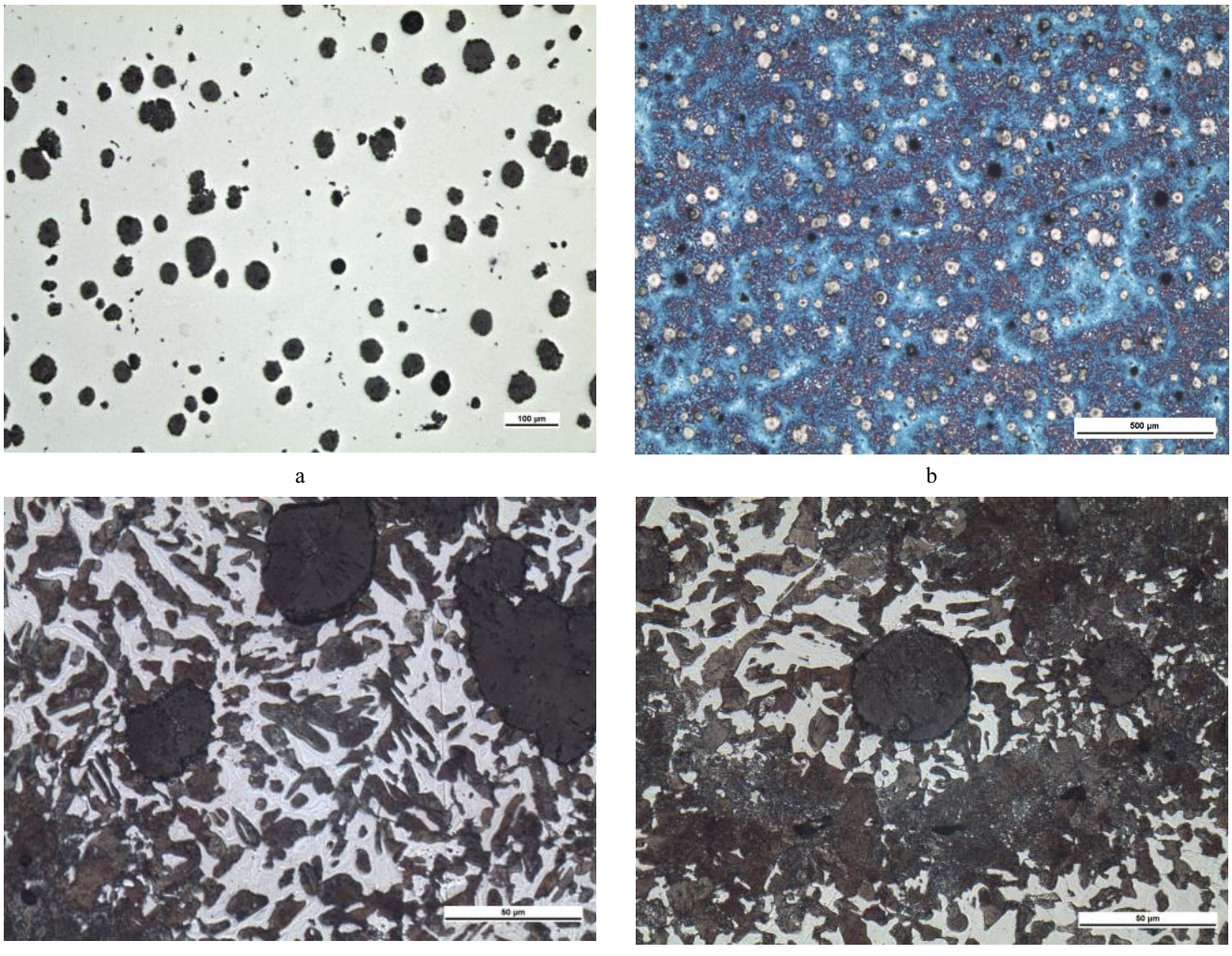

a b

c d

Fig. 1. Perferritic IDI: a – graphite nodules, non-etched; b – eutectic cells, etched with sodium chromate; c – characteristic microstructure, etched with 3 % Nital; d – pearlite on the borders of eutectic cells with presence of shrinkages, etched with 3 % Nital

The stress intensity factor amplitude K_a for the CT specimen geometry is given by:

$$\Delta K = \frac{\Delta P}{B\sqrt{W}} \frac{(2+\alpha)}{(1-\alpha)^{3/2}} \cdot \cdot \left(0.886 + 4.64\alpha - 13.32\alpha^2 + 14.72\alpha^3 - 5.6\alpha^4\right), \quad (2)$$

$$\alpha = \frac{a}{W}, \quad (3)$$

where P_a [MPa] is the load amplitude; B [mm] is the specimen thickness; W [mm] is the specimen width and a [mm] is the crack size.

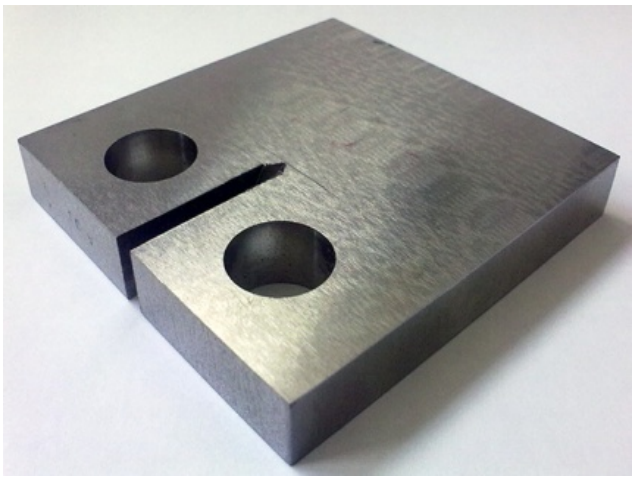

Fig. 2. Compact Tension (CT) specimen

The threshold stress intensity factor amplitude K_{ath} was determined using the load shedding technique [7]. This procedure involves slowly reducing the stress intensity factor amplitude by reducing stepwise the applied load after the crack had grown by at least 1 mm in length at the previous K_a level, and recording the crack growth rate da/dN. The crack growth threshold values K_{ath} were then identified as the values of K_a at which the crack growth rate was of the order of 10^{-10} m/cycle.

After fatigue crack propagation test, the CT specimens were broken under tensile load. Tensile properties of experimental material were measured on flat tensile testing specimens, extracted from the halves of CT specimens. Three identical tensile specimens were prepared from each CT halve. MTS 810 testing machine equipped with extensometer model 632.31F-24 was used to perform the tensile tests. Frequency of acquisition was 10 Hz, rate of test 0.01 mm/s and the load cell maximum load was 25 kN.

The structural analysis of local microstructure was carried out on polished cross-sections of tensile test specimens, etched with 3 % Nital. The graphite size was evaluated according to the standard EN STN 42 0461 and the range of graphite particles size indicates the number in the brackets according to the etalons. Quantitative analysis was performed in the light metallographic microscope NEOPHOT 32 with the metallographic software NIS Elements AR 3.00.

3. RESULTS AND DISCUSSION

3.1. Near-threshold fatigue crack growth

Fatigue crack propagation data of IDI determined on three identical CT specimens are shown in the bilogarithmic plot of Fig. 3. The data show a well-defined near-threshold region of fatigue crack propagation and the Paris law region.

The fatigue crack growth rate curves of Fig. 3 clearly show that the near-threshold behavior and K_{ath} are significantly different for the three specimens, while the fatigue crack propagation behavior tends a similar trend in the Paris law region.

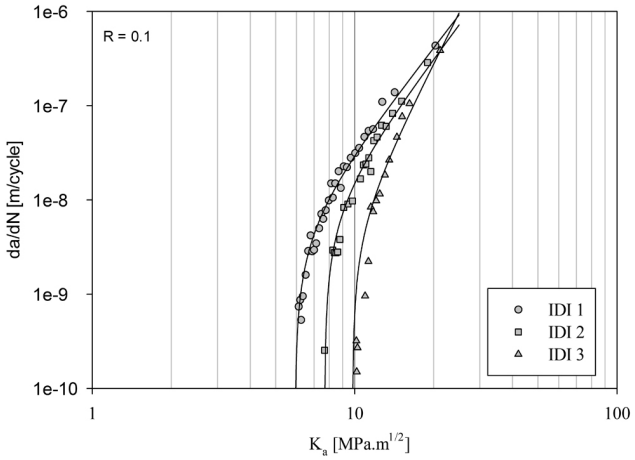

Fig. 3. Fatigue crack propagation data of perferritic IDI specimens, $R = 0.1$

Table 2 shows the values of the threshold stress intensity factor amplitude K_{ath} and the slopes m of the linear part of fatigue crack propagation curves.

Table 2. Fatigue crack propagation data

Specimen	K_{ath} [MPa·m$^{1/2}$]	m [slope]
IDI 1	5.93	3.59
IDI 2	7.68	3.73
IDI 3	9.81	5.54

It is widely believed that fatigue crack growth rate in the near-threshold regime is dominated by both intrinsic material features (such as composition, microstructure) and extrinsic testing conditions (e. g. test atmosphere and temperature, corrosive medium, load ratio and history, especially load ratio, overload and crack closure if available), [9 – 12]. In the Paris law regime, the crack growth rate becomes rather insensitive to material microstructure [13]. Since the testing environment for all three CT specimens was kept unchanged, i. e. dry ambient laboratory atmosphere, room temperature, and aspect ratio was kept constant $R = 0.1$, the further investigation was focused on local tensile properties and the character of local microstructure, to explain detected range of stress intensity factor amplitude K_{ath}.

3.2. Local tensile curves

Stress-strain curves, determined on three representative tensile specimens are shown in Fig. 4.

The reference data from the tests such as tensile strength, yield strength, Young's modulus of elasticity, elongation to rupture and Brinell hardness, respectively, are summarized in Table 3. In general, measured data show only minor differences. However, specimens IDI 2 and IDI 3 have fairly similar properties, while IDI 1 has

slightly higher tensile strength, yield strength and hardness and lower ductility.

Table 3. Hardness and tensile properties of IDI specimens

Specimen	R_m [MPa]	$R_{p0.2}$ [MPa]	E [GPa]	A [%]	HBW
IDI 1	778	476	156.2	6.9	223
IDI 2	753	429	151.6	7.6	210
IDI 3	757	439	145.2	7.5	208

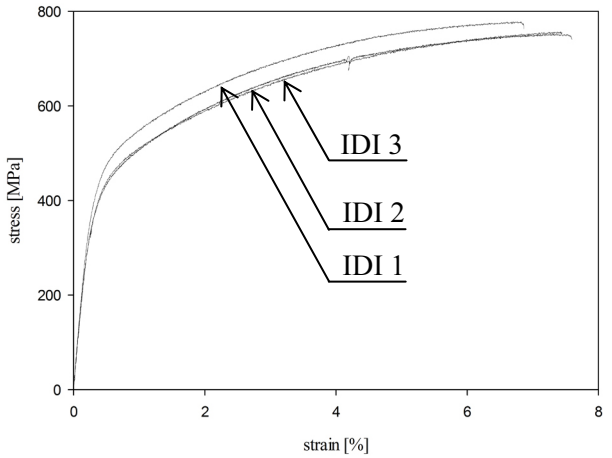

Fig. 4. Stress-strain curves determined on perferritic IDI specimens

3.3. Local microstructure analysis

Microstructure of perferritic IDI in representative cross-sections of the tensile specimen was examined using the techniques of quantitative metallography and nonconventional metallography methods such as color metallography. The results of the quantitative analysis are given in Table 4.

The microstructure of perferritic IDI specimens consisted of proeutectoid ferrite, perlite and nodules of graphite particles. The determined nodule count was in a range of (74 – 95) nodules/mm^2, with area fraction of 12 %, the same for all three specimens.

The size of nodules was predominantly in the range from 30 μm – 60 μm (6), with different ratio of nodules with size in the range of 15 μm – 30 μm (7) and of 60 μm – 120 μm (5). Comparing the area fraction of proeutectoid ferrite and pearlite within the microstructure, it is found that the matrix composition of IDI 2 and IDI 3 are similar, while the IDI 1 specimen shows slightly lower amount of proeutectoid ferrite and more pearlite. The slightly higher tensile strength, yield strength and hardness of IDI 1 specimen could be explained by the higher content of pearlite, whose lamellar structure of alternate layers of ferrite and cementite is characterized by high strength and ductility [1].

Fig. 5, a, b, shows the microstructure of IDI 1 and IDI 3 specimen respectively.

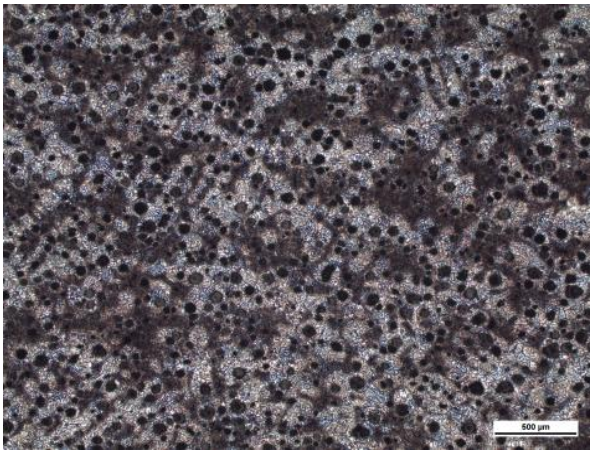

a

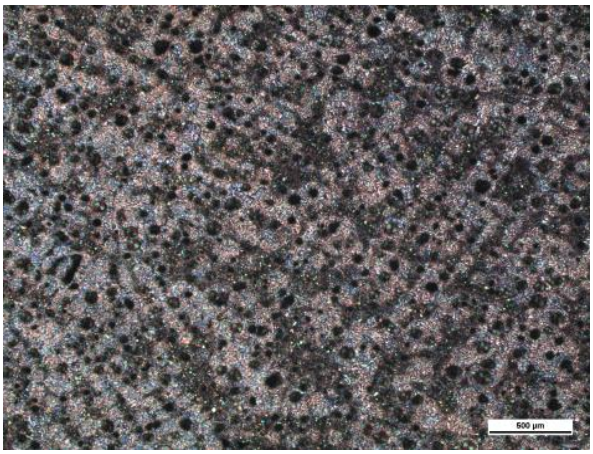

b

Fig. 5. Eutectic cells in perferritic IDI: a – specimen IDI 1; b – specimen IDI 3, Nomarski, etched with 3 % Nital

The microstructures of perferritic IDI specimens show only a partly uniform distribution of graphite particles within the matrix. The nodules of graphite are generally segregated in the centre of the region of eutectic cells surrounded by pearlite. Graphite is predominantly present in the proeutectoid ferritic fraction of the matrix, but occasionally can be found also in the region of pearlite or near the pearlite region, respectively.

The shape of proeutectoid ferrite within the matrix of IDI specimens is considered in Fig. 6. The matrix of IDI 1 specimen, Fig. 6, a, is characterized by lower amount of proeutectoid ferrite (area fraction is 29 %) segregated mainly in the thinner acicular form.

Table 4. Quantitative analysis of perferritic IDI microstructure

Specimen	Nodule count [mm^{-2}]	Nodule size	Nodules area fraction [%]	Proeutectoid ferrite area fraction [%]	Pearlite area fraction [%]
IDI 1	82	10 % 5 + 65 % 6 + 25 % 7	12	29	59
IDI 2	95	5 % 5 + 65 % 6 + 30 % 7	12	33	55
IDI 3	74	15 % 5 + 65 % 6 + 20 % 7	12	34	54

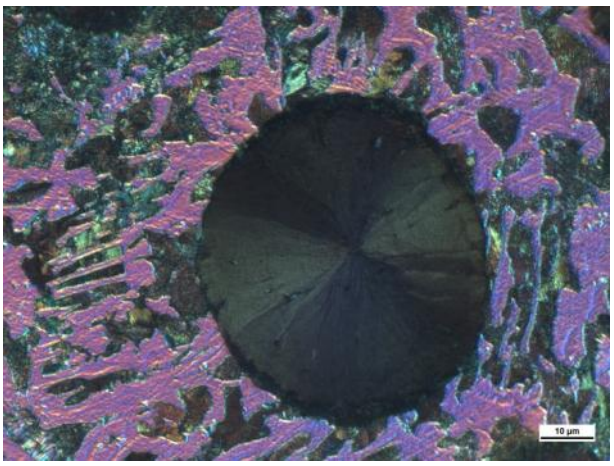

a

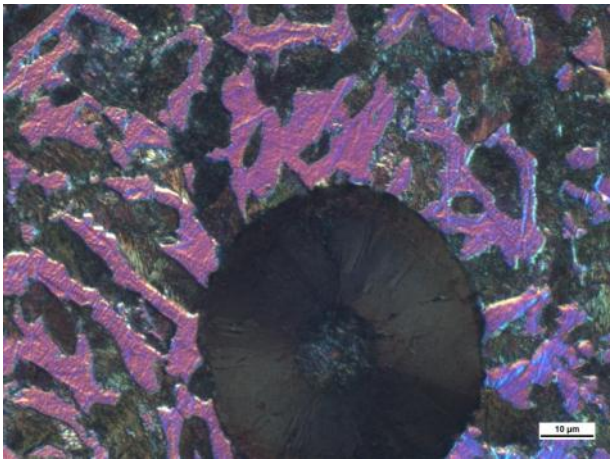

b

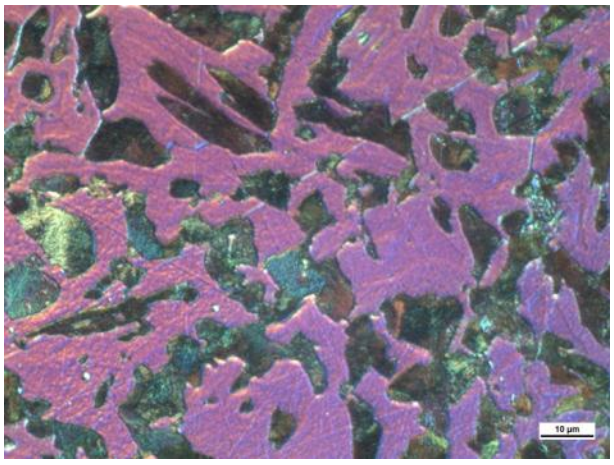

c

Fig. 6. Shape of proeutectoid ferrite in specimens: a – IDI 1; b – IDI 2; c – IDI 3, Nomarski, etched with 3 % Nital

In the case of IDI 2 and IDI 3 specimen, Fig. 6, b, c, the area fraction of proeutectoid ferrite is higher (33 % respectively 34 %) and it is segregated in coarser shape (i. e. polyedric grains) than for IDI 1.

4. CONCLUSIONS

Fatigue crack propagation curves, da/dN vs. K_a, and the threshold K_{ath} obtained for the present IDI specimens showed a significant specimen-to-specimen variability going from 6 MPa·m$^{1/2}$ to 10 MPa·m$^{1/2}$.

Tensile tests performed demonstrated that static properties may vary from place to place within a cast block of IDI.

A detailed microstructural characterization of different IDI specimens showed: i) substantial similarity in structural parameters; ii) a possibly significant inverse correlation of ferrite content in the matrix and static strength; iii) a direct correlation of ferrite content and threshold K_{ath}.

Acknowledgments

Authors would like to thank to national project VEGA 1/0242/10 for support of experimental research.

REFERENCES

1. **Davis, J. R.** Cast Irons ASM Specialty Handbook. ASM International, 1996: 494 p.
2. **Harding, R. A.** The Production, Properties and Automotive Applications of Austempered Ductile Iron *Kovove Materialy* 45 (1) 2007: pp. 1 – 16.
3. **Hayrynen, K. L.** The Production of Austempered Ductile Iron (ADI) *2002 World Conference on ADI* Louisville (KY) Ductile Iron Society and the American Foundry Society 2002.
4. **Massagia, S.** The Development of ADI and IDI in Italy *Procedia Engineering* 2 (1) 2010: pp. 1459 – 1476.
5. **Lee, Y. L., Pan, J., Hathaway, R. B., Barkey, M. E.** Fatigue Testing and Analysis: Theory and Practice. Butterworth-Heinemann, 2005: 402 p.
6. **Bokůvka, O., Nicoletto, G., Kunz, L., Palček, P., Chalupová, M.** Low and High Frequency Fatigue Testing. EDIS, Žilina, 2002: 100 p.
7. ASTM Standard E 647-08: Standard Test Method for Measurement of Fatigue Crack Growth Rates, 2009.
8. **Rivera, G. L., Boeri, R. E., Sikora, J. A.** Revealing and Characterising Solidification Structure of Ductile Cast Iron *Materials Science and Technology* 18 (6) 2002: pp. 691 – 697.
9. **Sadananda, K., Vasudevan, A. K.** Fatigue Crack Growth Mechanisms in Steels *International Journal of Fatigue* 25 (9 – 11) 2003: pp. 899 – 914.
10. **Choi, Ch., Kim, H. J., Lee, Y. T., Kim, Y. W., Lee, Ch. S.** Effect of Microstructural Parameters on the Fatigue Crack Growth of Fully Lamellar γ-TiAl Alloy *Materials Science and Engineering: A* 329 – 331 2002: pp. 545 – 556.
11. **Fonte, M. A., Stanzl-Tschegg, S. E., Holper, B., Tschegg, E. K., Vasudévan, A. K.** The Microstructure and Environment Influence on Fatigue Crack Growth in 7049 Aluminum Alloy at Different Load Ratios *International Journal of Fatigue* 23 (1) 2001: pp. 311 – 317.
12. **Kumai, S., Hu, J., Higo, Y., Nunomura, S.** Effect of Dendrite Cell Sizy and Particle Distribution on the Near-threshold fatigue Crack Growth Behaviour of Cast Al-SiCp Composites *Acta Materialia* 44 (6) 1996: pp. 2249 – 2257. http://dx.doi.org/10.1016/1359-6454(95)00357-6
13. **Yang, J., Putatunda, S. K.** Near Threshold Fatigue Crack Growth Behaviour of Austempered Ductile Cast Iron (ADI) Processed by a Novel Two-step Austempering Process *Materials Science and Engineering: A* 393 (1 – 2) 2005: pp. 254 – 268.

Presented at the 20th International Baltic Conference "Materials Engineering 2011"
(*Kaunas, Lithuania, October 27–28, 2011*)